Multi-Modal Artificial Intelligence in Additive Manufacturing: Combining Thermal and Camera Images for 3D-Print Quality Monitoring

Markus Bauer[1,*], Benjamin Uhrich[2,*], Martin Schäfer[3], Oliver Theile[3], Christoph Augenstein[2] and Erhard Rahm[2]

[1]*Institute for Applied Informatics, Goerdelerring 9, Leipzig, Germany*

[2]*Center for Scalable Data Analytics and Artificial Intelligence, Humboldtstraße 25, Leipzig, Germany*

[3]*Siemens AG, Siemensdamm 50, Berlin, Germany*

Keywords: Artificial Intelligence, Additive Manufacturing, Physics-Informed Neural Networks, Multi-Modal Imaging, Quality Monitoring.

Abstract: With emerging technologies such as high-precision Laser Powder Bed Fusion (LPBF), rapid prototyping has gained remarkable importance in metal manufacturing. Furthermore, cloud computing and easy-to-integrate sensors have boosted the development of digital twins. Such digital twins use data from sensors on physical objects, to improve the understanding of manufacturing processes as a whole or of certain production parameters. That way, digital twins can demonstrate the impact of design changes, usage scenarios, environmental conditions or similar variables. One important application of such digital twins lies in early detection of manufacturing faults, such that real prototypes need to be used less. This reduces development times and allows products to be individually, affordable, powerful, robust and environmentally friendly. While typically simple USB-camera setups or melt-pool imaging are used for this task, most solutions are difficult to integrate into existing processes and hard to calibrate and evaluate. We propose a digital-twin-based solution, that leverages information from camera-images in a self-supervised fashion, and creates a heat transfer based AI quality monitoring. For that purpose, artificially generated labels and physics simulation were combined with a multi-sensor setup and supervised learning. Our model detects printing issues at more than 91% accuracy.

1 INTRODUCTION

The virtual world of development, testing, and optimization of complex products and processes nowadays precedes production processes in the real world. Future components and operations are created and simulated as software models – a so-called digital twin. Digital twins are virtual equivalents of products, machines, processes, or even entire production plants that contain all relevant data and simulation models. To ensure precise simulation throughout the life of a product or its production, digital twins use data from sensors on physical objects, to determine real-time performance, operating conditions, and changes to the system over time. By incorporating multi-physics simulation, data analysis and machine learning capabilities, digital twins can demonstrate the impact of design changes, usage scenarios, environmental conditions or similar variables. Hence, excessive usage of real prototypes is avoided, which offers advantages in cost reduction and sustainability.

In the special case of metal additive manufacturing (MAM), avoiding faulty prints is a crucial factor, especially for the case of rapid prototyping, where production time and material usage are key performance indicators, and must be kept low. Furthermore, the influence of misjudged printing parameters such as laser power must be reduced, to make a valid estimate of the final product's quality, based on the prototypes. Digital twins are an adequate option, to build up a quality monitoring, that ensures a high standard throughout the MAM process. Hence, they have gained popularity in MAM.

Recent work has shown, that AI can support the simulation of complex physical processes such as fluid dynamics and heat transfer, which are of con-

[*]M. Bauer and B. Uhrich contributed equally to this work as first authors.

Bauer, M., Uhrich, B., Schäfer, M., Theile, O., Augenstein, C. and Rahm, E.
Multi-Modal Artificial Intelligence in Additive Manufacturing: Combining Thermal and Camera Images for 3D-Print Quality Monitoring.
DOI: 10.5220/0011967500003467
In *Proceedings of the 25th International Conference on Enterprise Information Systems (ICEIS 2023) - Volume 1*, pages 539-546
ISBN: 978-989-758-648-4; ISSN: 2184-4992

siderable relevance for successfully printing layers in MAM without issues such as porosity. This especially accounts for the use of physics-informed neural networks (PINNs), which have been shown to provide competitive simulation results to standard approaches such as the finite element method (FEM) (Zhu et al., 2021). In addition, there is a large trend in fusing multiple sources of information in a single AI model, which aids in manufacturing applications that typically utilize multiple sensors of different types. Another recent development in AI is the use of self-supervised models that can significantly reduce the training effort, by superseding the need for manual annotation.

In this work, we are using AI methods, to demonstrate how a quality monitoring can be implemented, without the need for time- and cost expensive sensor setups and manual data analysis. Our approach aims for applicability in small to medium enterprises, where access to specialist equipment (such as CT- or X-ray scanners) often is limited, and labelling procedures (required for supervised AI approaches) are unfeasible, as it would require too much time of highly skilled experts. For our solution, we thus create print quality pseudo labels in a self-supervised fashion using only one reference build part (BP) and a simple USB-camera together with an autoencoder model. We then proceed to combine the pseudo labels with the output of a PINN that was applied to a pyrometer's measurements, to build a BP-quality-classifier. Our model achieves state-of-the-art results as presented in section 4.

To the best of our knowledge, our approach is the first leveraging physics simulation, high-speed camera imaging and AI together with widespread, inexpensive sensor setups for high accuracy error detection. The contribution of our work are as follows:

- We present a setup, which is easy to integrate, inexpensive, and thus is a feasible solution for small to medium enterprises (SMEs).
- We use a self-supervised autoencoder to create labels for classification as high, medium and low-quality layers, whereas data exploration is reduced to evaluating few representative samples.
- We demonstrate the use of PINNs for quality assurance in LPBF processes.
- We show that pseudo labels taken from camera-images and thus reflecting the BP's quality can be used to directly build a classifier upon highly informative temperature field information. This way, the model may be used to identify critical parts in the temperature field images and then refined to more sophisticated models.

2 RELATED WORK

To understand the scientific background of our proposed solution, related work in the domains of MAM and AI needs to be considered. In this section, relevant literature is provided, to gain a good overview of the work's fundamentals.

2.1 Metal Additive Manufacturing

Recently, MAM has experienced a significant upswing, as it offers great potential in reducing the effort required to build metal parts. This can be especially useful where iterative development of certain parts is required, for example in the field of rapid prototyping. Several efforts have been made in MAM monitoring and computer-assisted process controlling by various scientific and industry teams. To this end, Praveena *et al.* provide a comprehensive review of MAM, particularly on methods, applications, materials, challenges, trends and future potentials (Praveena et al., 2022). Nevertheless, MAM is a highly complex process, that requires controlling of various parameters such as laser-power, scan velocity etc. (Knaak et al., 2021). Additionally, melting and fusing metal leads to heating and cooling cycles that significantly affect component quality. A research milestone in the field of numerical simulation from Mukherjee *et al.* made it possible to get a more in-depth understanding of heat and fluid flow in MAM (Mukherjee et al., 2018).

2.2 Machine Learning

Due to AI's increasing popularity, various conceptualizations have been proposed for automated or AI-driven quality assurance in MAM. The most popular approaches extract their information from melt pool images or characteristics (Akbari et al., 2022; Kunkel et al., 2019) or high-speed camera setups (Kwon et al., 2018). Promising results could be achieved that way. For example, Kunkel *et al.* (Kunkel et al., 2019) achieve an accuracy of 99.7% in classifying four categories of yield strength (good, average, bad, and mapping failure). Inspired by the success of analytic approaches that operate on melt pool shape or layerwise camera-imaging, recent work includes setups that combine multiple domains for even better model accuracies. Shen *et al.* (Shen et al., 2022) propose a system for weld reinforcement. Their solution includes multi-modal information given by the melt pool camera images, as well as heatmap images of different parameter groups.

We adapt the basic ideas and core findings of the

referenced work and transfer them to our use case. In addition, we extend the existing approaches, by paying particular attention to self-supervised learning and heat flow simulation, to achieve comparable results with less effort on the industry-practitioner side.

2.2.1 Autoencoder

Autoencoders (AEs) consist of two phases, the encoding step and the decoding step. In the encoding step, a non-linear function is learned that transforms the input into a low-dimensional vector space, and in the decoding step, an inverse transformation is learned that reconstructs the input from this low-dimensional vector space. AEs are an effective method for detection of anomalies in unlabelled data. Bel-Hadj *et al.* presented an AE for anomaly detection in vibration signals for structural health monitoring of an offshore wind turbine (Bel-Hadj and Weijtjens, 2023). The principle also works in physics, as Ngairangbam *et al.* have recently shown in an application using a quantum AE (Ngairangbam et al., 2022).

In our case, autoencoders are used as a tool to automatically extract print quality labels from diverging representations of different BP's layers, which is a scenario comparable to referenced works.

2.2.2 Physics-Informed Neural Networks

Heat transfer during melting in 3D printing is one of the most important factors influencing part quality in MAM. To monitor MAM processes, heat transfer must be considered and understood. Such a natural phenomenon based on physical laws is well known. Researchers have been studying thermal behaviour more than 100 years and have formalized their knowledge in the form of partial differential equations (PDEs). There is an opportunity to incorporate this knowledge into classical deep learning algorithms such as neural networks (NNs) to increase prediction accuracy with the data-driven capabilities of NNs. Raissi *et al.* were the first to show that PINNs are a viable alternative method to obtain an approximation for solving these PDEs, using several time-dependent benchmark problems (Raissi et al., 2019). A good overview of the possibilities of PINNs for heat transfer problems is given by Cai *et al.* (Cai et al., 2021). Zhu *et al.* presented first results for heat transfer and fluid flow in MAM using PINNs and compare the solutions with finite element method.

PINNs are used in our work to generate input for the error classifier. We assume that deviations between the estimated temperature profiles and the measured ones will help to indicate emerging problems such as delamination. As PINNs embed existing physical knowledge, possibly more meaningful information can be supplied than using just the raw data.

2.2.3 Multi-Modal Machine Learning

Multimodal ML is important if there is more than one data representation or modality for the same real-world application, respectively. This could be the combination of text and images or images of different types, such as greyscale and thermal images. Similar to our work, Gaikwad *et al.* (Gaikwad et al., 2020) incorporate information from a pyrometer as well as a high speed video camera to characterize the quality of single tracks printed using LPBF. They extract various statistical features for each sensor measurement and process them using a set of echelon artificial neural networks. Using quality metrics generated from profilometer measurements, their approach provides state-of-the-art results for detecting and pairing errors (e.g., balling, keyholding) to critical process parameters (e.g., laser velocity and laser power). More recent work of the authors (Gaikwad et al., 2022) on the effects of melt pool characteristics (e.g., temperature, spatter, and size) on build part porosity presents a similar approach. The main difference to our work lies in the more time-, knowledge- and resource expensive setup, which may be impractical for small to medium enterprises.

As described in section 4, multi-modal machine learning is a good strategy to increase the performance of a printing error classifier. We thus make use of this technique in our work.

3 METHODS

Our proposed architecture features the application of supervised CNN learning, Autoencoders for label-generation and process simulation using PINNs. Below, those methods' theoretical background is provided.

3.1 Laser Powder Bed Fusion

For our experiments, we use the LPBF procedure, which is one of the most widespread and industrially used additive manufacturing processes. It is based on the melting of single metal powder layers using a laser beam. The laser energy is focused on the powder surface and the powder is melted at the focal point due to the high energy-density. The laser "scans" the geometric shape of the component to be produced in each powder layer, i.e., the laser beam is deflected by a mirror system and the focal point is guided over the pow-

der surface according to a predefined pattern. After melting a layer, the build platform is lowered, usually approx. 50 μm, powder is reapplied through a recoating system and afterward the next layer is melted. The laser energy is sufficient to create a melt pool that extends over several layer thicknesses. However, the resulting melt pool must be adapted to both the material and the process settings to ensure optimal, true-to-shape solidification of the metal without defects such as cracks or flaws. It is thus similar to the welding process, but more complex, as not only individual traces are melted, but flat areas besides small zones are created without interruptions. The melting and cooling behaviour of the process is more comprehensive and dependent on a variety of process conditions.

3.2 Multimodal Dataset

To develop and test a real-time data processing workflow, EOS M 290 and SLM 280 laser melting machines were used. In total, nine different specimens of pillars have been built in two distinct print jobs with AISI 316L (1.4404), and IN718 (2.4668) powder. For each print job, 382×288 pixels greyscale images and pyrometer heatmaps of $\lambda = 7\,\mu$m to $14\,\mu$m were recorded with $f_{record} = 3$ Hz. While for the first job only smaller printing errors could be observed qualitatively, the second print job contained significant warping / delamination issues. The quality of the first build job was evaluated by manufacturing experts, using surface roughness and shape deviation measurements, and found to be on a par with the manufacturer's quality standards. For the second build job, no further part evaluation was done, as severe issues were clearly visible.

3.3 Machine Learning Methods

Multiple machine learning methods have been applied, to create the error classifier, including an autoencoder, PINNs and convolutional neural networks (CNNs) trained with supervision.

An Autoencoder, as described in section 2.2.1 is a special kind of NN that uses an encoder E to create vector representations z (:= embeddings) from input data X (i.e., camera images), and a decoder D to restore the original images. The output image $\hat{X}$ thus is created by:

$$\hat{X} = D(z \sim E(X, \omega), \theta) \tag{1}$$

where ω refers to the encoder's and θ to the decoder's parameters. As the decoder is simply the inverse of the encoder, weights can be shared between them. In this case, ω is identical with θ. For training, a reconstruction error between X and $\hat{X}$ is calculated and used to optimize the parameters ω of the network by solving:

$$argmin_{\omega,\theta} \frac{\sum(X - \hat{X})^2}{N} \tag{2}$$

with N as the total number of input samples. The created embeddings z can then, as in our case, be used as pseudo labels to train further models, or directly to perform tasks like clustering etc.

PINNs describe a special form of NNs that incorporate PDEs as a mathematical formalism of knowledge about physical behaviour. A neural network is trained to learn a function $T_{NN}(t,x,y,z,W,b)$ that can approximate a scalar temperature field while considering the energy conservation equation. t,x,y,z describes the spatial-temporal domain of the BP and W, b are the trainable weights and bias of the neural network. The optimization of the weights and biases W, b are driven by initial and boundary value conditions as well as by the PDE of energy conservation. If any of the three restrictions is not satisfied, this is penalized in the form of the loss function (3) and optimized by backpropagation.

$$Loss = \lambda_1 R_1 + \lambda_2 R_2 + \lambda_3 R_3 \tag{3}$$

Here R_1 and R_2 are initial and boundary conditions, and R_3 describes the energy conservation equation. To obtain the derivatives of the learned function T_{NN}, automatic differentiation is used. $\lambda_1 - \lambda_3$ are weights of the individual loss terms, ranging from 0-1, prioritizing the loss terms differently. Using the pseudo labels created from the autoencoder and the images created with the PINNs, a CNN $M(X, \psi)$ is trained in a supervised fashion. This is done by optimizing the parameters ψ using the cross entropy loss between the outputs of M and the pseudo labels $\hat{X}$.

3.4 Proposed Training Architecture

To create an error classification model, we are using a procedure as depicted in Fig. 1. We are combining both the thermal and greyscale records in the created dataset. For that purpose, first, we train an autoencoder to a set of hold-out patches taken from the successful BPs greyscale images, with the objective to reduce the mean squared error of the reconstruction vs. the input image.

The greyscale data consists of 110×110 pixels patches x and x_{ref} (15112 patches in total), cropped from the full-size images, around the individual pillar's centre. Additionally, as the pillars are of different shape and thus may never fill the whole image patch area, the final row of pixels was repeated to the edge

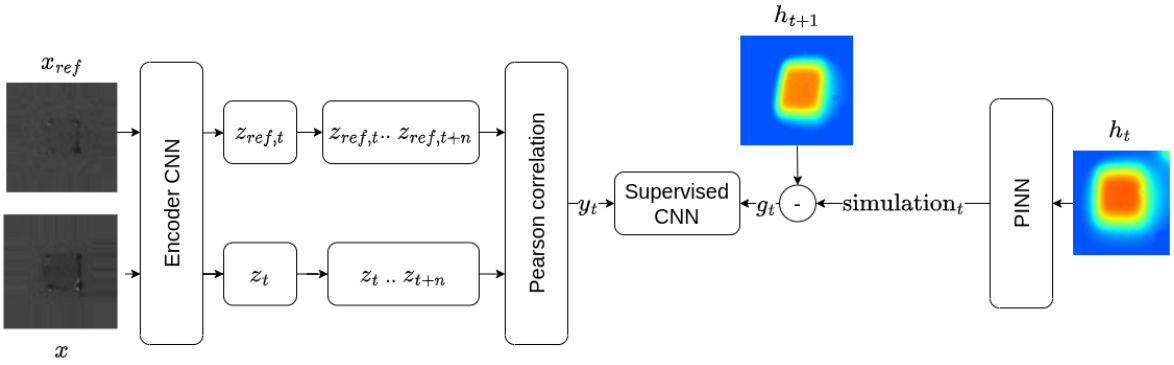

Figure 1: **Architecture of the proposed training method** - Camera images x_t are collected and processed using a NN encoder, together with a reference image. After buffering a certain number of images, a pseudo label is created using the Pearson correlation between reference and current images. As soon as pseudo labels y_t are created for a layer, referring images g_t are provided, which are created by subtracting the currently predicted temperature profile from the measured temperature field image. That way, a neural network is trained, to later predict, whether a layer was printed successfully.

of the patch according to the actual build parts shape, rather than applying zero padding. Our autoencoder uses a Resnet18-like architecture (He et al., 2016) for the encoder and decoder.

With the trained encoder, we then process the remaining images of both BPs to create a vectorized version z and z_{ref} of each patch, whereas z are the vectors of the faulty BP and z_{ref} are the ones of the successful BP. Afterwards, all vectors are stored in buffers of length $n = 10$ and compared using the Pearson correlation. That way, we identify trends of difference between the BPs, without any human supervision. With this procedure, except for an initial amount of 10 layers, we create pseudo labels y according to the following rule:

$$y = \begin{cases} \text{successful}, & \text{Pearson r} >= 0 \\ \text{warning}, & 0 > \frac{\partial \text{Pearson r}}{\partial t} > -0.02 \\ \text{failed}, & \text{otherwise} \end{cases} \quad (4)$$

The thresholds for the pseudo labels have been set empirically.

In the next step, we create input images g for training the classifier M. For that purpose, regions of the pillars are cropped from the heatmap images. We then create heatmap predictions h for each next layer, starting with the $n-1_{th}$ layer (as we already needed to discard images for greyscale images). We then subtract the heatmaps $simulation_t$ predicted from h_t from the previously measured ones h_{t+1} and take the absolute error to create a new training image g_t.

4 RESULTS

To create our model, we are running three distinct tasks. Those consist of training the PINN and AE, creating labels and images, and finally creating the classifier. Our particular results for each step are presented below.

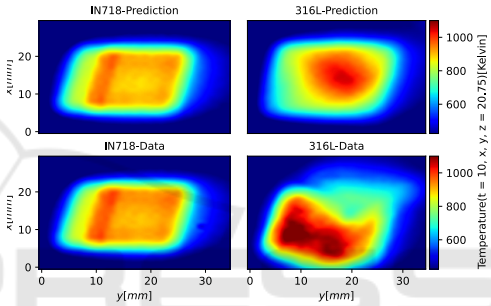

Figure 2: **Comparison of heat prediction** - Heat prediction for INC 718 (left) and 316L (right) in comparison with measurement data. For the INC718 print job prediction and measurement data match. In the case of the 316L print job prediction and measurement data show differences indicating defective layers, as the simulations match, i.e., layers that have been printed earlier.

4.1 Heatmap Simulation

Heatmap prediction is based on a fully connected, physics-informed feed forward network. Each printed layer is simulated by solving an initial and boundary value problem. The NN is informed by the energy conservation equation, which describes the physical laws of heat transfer, and the solution domain is described by randomly selected collocation points. On these points, a solution is prepoints, based on a batch size of 1000. We set initial and boundary conditions based on real measured data. For this purpose, a training data set of a total of 1200 thermal images was used for the entire printing process. Additionally, a heat source position detection method is implemented to produce comparable heatmaps. The heat source

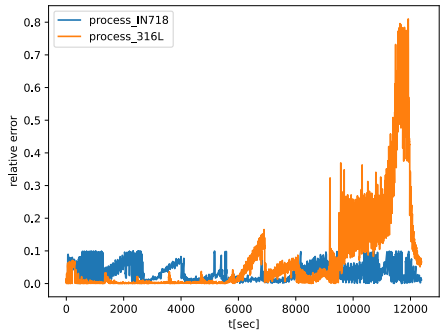

Figure 3: **Error between temperature scalar field of prediction and sensor data** - To quantify anomalies, the relative error between prediction and sensor data is calculated over more than three hours of printing. Irregularities can be detected, especially in the last section of 316L.

is described analytically by a Gaussian function. A sigmoid function was used as an activation function in each layer and a learning rate of 10^{-3}. Fig. 2 shows an example solution of a heatmap prediction for a specific point at a time t. For the nickel-based alloy INC718, the heatmap simulation is comparable to the measured data of the print job. For the 316L stainless steel, the heat simulation and the measured data are not equivalent, significant disparities are visible. Boundary conditions are not met, and heat build-up can be seen, affecting BP quality. These anomalies can be quantified, as can be seen in Fig. 3. The distance between the scalar field of the temperature measurement and the simulation is calculated and quantified using the relative error over a printing duration of more than three hours. Significant differences between the simulation and the measurements can be seen, especially in the fourth quarter.

4.2 Generated Pseudo Labels

The heatmap difference images g are matched with the labels y to create a dataset of 37246 data pairs. As the pyrometer-based data was recorded using a higher sampling rate than the greyscale images, the same label y_t has been used for a layer's heatmap images, according to the timestamp of the greyscale images. The data was split into a training and test set, whereas separate layers were used in the subsets to avoid overfitting. Fig. 4 shows some example images taken from g. From the examples, it's evident, that distinguishing successful and failed layers can be a challenging task, when considering the deviations in the simulated and measured temperature profile. A plausible way to interpret the data, may be that the temperature differences are generally low for successfully printed layers. In case a faulty layer or multi-layer area of the BP is emerging, anomalous temperature spread is risking especially at the corners of the BPs, which is the case for the warning class. By the time a faulty layer can even be identified by human supervision, the temperature profile shows larger deviations in the area where the BP is melted. It is, however, hard to draw a clear border here. Thus, using self-supervised learning as a label generator and an AI-based approach to build a classifier is a promising approach, that enables manufacturers to create a fault prevention based on heatmap data.

Table 1: **Performance of different classification models** - Evaluation were done using balanced accuracy (Acc.) and f_1 scores for successful (s), warning (w), and failed (f).

Model	Acc.	$f_{1,s}$	$f_{1,w}$	$f_{1,f}$
Resnet18	0.917	**0.98**	0.87	0.89
Resnet50	0.920	**0.98**	0.87	**0.90**
EfficientNet-B0	**0.926**	**0.98**	**0.88**	0.89
MobileNet-V3	0.860	0.96	0.79	0.81

4.3 Printing Error Classifier

With the created dataset, we proceed to train a supervised CNN. We use a learning rate of $5 \cdot 10^{-6}$, a weight decay of $1 \cdot 10^{-7}$, and a cyclic learning rate. We evaluated the Resnet18, Resnet50 (He et al., 2016), EffcientNet-B0 (Tan and Le, 2019) and MobileNet-V3 (Howard et al., 2017) architectures, together with 2D batch norm layers and Dropout of 0.1 for each convolution layer, which were pretrained to the ImageNet dataset (Deng et al., 2009). The image size was downsampled to 35×35 pixels, with a batch size of 256. The cross entropy loss was used as a cost function. We train the model until the point of convergence, which is determined as the intersection of the training and validation loss curve. After training the model, classification accuracy was measured using the test data and within a 5-fold cross validation scenario. A maximum accuracy of 92.60% was achieved this way by a EfficientNet-B0 (c.f. Tab. 1), which even improves earlier work of the authors (Bauer et al., 2022). For most of the individual classes' f_1 scores, the EfficientNet-B0 performs best as well, even though the residual networks achieve comparable performance.

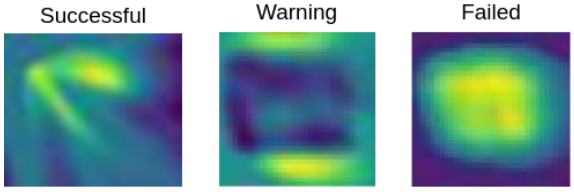

Figure 4: **Example images** - of a successful layer (left), a layer that causes a warning (centre), and a faulty layer (right).

Further investigation indicated that most confusion occurs for failed layers that have been marked as successful. The successful layers, on the other hand, have been classified very well. The most confusion only occurred to the warnings, which are not critical for practice. It should be noted that the earlier layers recorded consist of support material, which may mislead the classifier, given the fact that only few such examples are provided. Additionally, outliers in the self-supervised labelling procedure can impose a degree of label noise, which can't be avoided completely. Thus, the number of missed errors can be expected to be lower than in Tab. 1, in practice.

In a real-world application, however, a false negative for an actually faulty layer may cause severe issues within the production. The warning class serves as a measure against missing faulty layers completely, by smoothing the borders between *successful* and *failed*. The high $f_{1,w}$ value (c.f. Tab. 1) indicates that the warning class compensates most of the successful as failed / failed as successful false positives. This would reduce the amount of manual inspection, as well as "false alarms" in practice.

The model's performance can be demonstrated better, by visually investigating how certain cases have been classified, as depicted in Fig. 5. The example underlines the model's capability of fine-granular separation of different temperature profile types. For example, the first and last image look very similar, but show indeed a successful and failed layer. The model successfully classifies both of them right, even with a high probability. Confusion with the *successful* class, as described above, often occurs during the support layer printing. The model's predictions thus seem plausible.

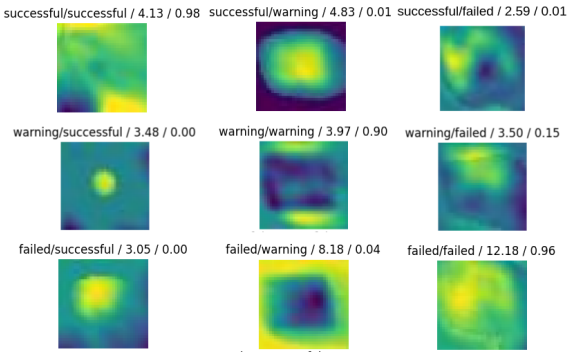

Figure 5: **Example temperature difference images** – and the model's referring prediction (actual/prediction/loss/probability) for low model loss.

5 DISCUSSION

Summarizing, it could be shown that the presented approach successfully can be used to predict a BPs current quality, using example components. We achieve a competitive accuracy in this task using various AI methods. Our approach has potential to increase AM production quality, while keeping efforts for manufacturers low, as only few resources are needed for implementation.

For a more general approach, however, extensive evaluation needs to be done on other components, especially on such with different and more complex geometries. The transferability of the approach to other metal powder has not yet been demonstrated. Further experiments should be conducted to determine the limitations of the proposed approach, when the material parameters, and thus the material behaviour itself, change. Furthermore, the problem with the initially printed support layers has to be clarified and has not been solved in this work so far. This will be investigated in a further approach. Possibly, the solution can be found in an additional model trained on the support layers. If the data quality can be improved, especially for the greyscale images, a more detailed analysis of the BP would be possible.

6 CONCLUSIONS AND FUTURE WORK

In this paper, we presented an approach, to build a simple AI-based error prevention, that combines multiple modalities of sensors. The created model can be used to digitally clone the actual BP's printing procedure, and to predict its current state. It therefore serves as a first digital twin part for in-process quality assurance. We conclude that extracting relevant information about BP quality from measured temperature profiles may be difficult, but of value for various quality monitoring models. To avoid the need for laborious annotation procedures, self-supervised learning may be used with more comprehensive prediction examples based on greyscale image data. In the future, issues, such as the remaining failed-as-successful classification should be investigated and reduced, to make the model a robust variant for practical use. Besides that, different usage scenarios may be investigated. This includes the mapping of AI and temperature profiles using different material properties after the print. As in the presented examples, self-supervised learning may be a good starting point here as well. Another important aspect is the application of such a monitoring tool as a trigger for a machine con-

troller. For example, errors could be minimized, if the laser power is reduced by the time of a warning, or at least if an error occurs. This would likely lead to an improved BP quality and thus should be investigated. Additionally, machine learning should be used to integrate more parts of a complete digital twin, such as geometry optimization and material planning. Summarizing, the presented approach is a vital proof of concept for the feasibility of moving AI into practice without too many expenses and labour time.

ACKNOWLEDGEMENTS

All results presented refer to the TWIN project (https://websites.fraunhofer.de/TWIN), funded by the Federal Ministry of Education and Research, Germany (02K18D052).

REFERENCES

Akbari, P., Ogoke, F., Kao, N.-Y., Meidani, K., Yeh, C.-Y., Lee, W., and Farimani, A. B. (2022). MeltpoolNet: Melt pool characteristic prediction in metal additive manufacturing using machine learning. *Additive Manufacturing*, 55:102817.

Bauer, M., Augenstein, C., Schäfer, M., and Theile, O. (2022). Artificial intelligence in laser powder bed fusion procedures – neural networks for live-detection and forecasting of printing failures. *Procedia CIRP*, 107:1367–1372. Leading manufacturing systems transformation – Proceedings of the 55th CIRP Conference on Manufacturing Systems 2022.

Bel-Hadj, Y. and Weijtjens, W. (2023). Anomaly detection in vibration signals for structural health monitoring of an offshore wind turbine. In Rizzo, P. and Milazzo, A., editors, *European Workshop on Structural Health Monitoring*, volume 270 of *Lecture Notes in Civil Engineering*, pages 348–358. Springer International Publishing, Cham.

Cai, S., Wang, Z., Wang, S., Perdikaris, P., and Karniadakis, G. E. (2021). Physics-informed neural networks for heat transfer problems. *Journal of Heat Transfer*, 143(6).

Deng, J., Dong, W., Socher, R., Li, L.-J., Li, K., and Fei-Fei, L. (2009). Imagenet: a large-scale hierarchical image database. In *2009 IEEE conference on computer vision and pattern recognition*, pages 248–255. IEEE.

Gaikwad, A., Giera, B., Guss, G. M., Forien, J.-B., Matthews, M. J., and Rao, P. (2020). Heterogeneous sensing and scientific machine learning for quality assurance in laser powder bed fusion – a single-track study. *Additive Manufacturing*, 36:101659.

Gaikwad, A., Williams, R. J., de Winton, H., Bevans, B. D., Smoqi, Z., Rao, P., and Hooper, P. A. (2022). Multi phenomena melt pool sensor data fusion for enhanced process monitoring of laser powder bed fusion additive manufacturing. *Materials & Design*, 221:110919.

He, K., Zhang, X., Ren, S., and Sun, J. (2016). Deep residual learning for image recognition. In *2016 IEEE Conference on Computer Vision and Pattern Recognition (CVPR)*. IEEE.

Howard, A. G., Zhu, M., Chen, B., Kalenichenko, D., Wang, W., Weyand, T., Andreetto, M., and Adam, H. (2017). Mobilenets: Efficient convolutional neural networks for mobile vision applications.

Knaak, C., Masseling, L., Duong, E., Abels, P., and Gillner, A. (2021). Improving build quality in laser powder bed fusion using high dynamic range imaging and model-based reinforcement learning. *IEEE Access*, 9:55214–55231.

Kunkel, M. H., Gebhardt, A., Mpofu, K., and Kallweit, S. (2019). Quality assurance in metal powder bed fusion via deep-learning-based image classification. *Rapid Prototyping Journal*, 26(2):259–266.

Kwon, O., Kim, H. G., Ham, M. J., Kim, W., Kim, G.-H., Cho, J.-H., Kim, N. I., and Kim, K. (2018). A deep neural network for classification of melt-pool images in metal additive manufacturing. *Journal of Intelligent Manufacturing*, 31(2):375–386.

Mukherjee, T., Wei, H. L., De, A., and DebRoy, T. (2018). Heat and fluid flow in additive manufacturing—part i: Modeling of powder bed fusion. *Computational Materials Science*, 150:304–313.

Ngairangbam, V. S., Spannowsky, M., and Takeuchi, M. (2022). Anomaly detection in high-energy physics using a quantum autoencoder. *Physical Review D*, 105(9).

Praveena, B., Lokesh, N., Abdulrajak, B., Santhosh, N., Praveena, B. L., and Vignesh, R. (2022). A comprehensive review of emerging additive manufacturing (3d printing technology): Methods, materials, applications, challenges, trends and future potential. *Materials Today: Proceedings*, 52:1309–1313.

Raissi, M., Perdikaris, P., and Karniadakis, G. E. (2019). Physics-informed neural networks: A deep learning framework for solving forward and inverse problems involving nonlinear partial differential equations. *Journal of Computational Physics*, 378:686–707.

Shen, B., Lu, J., Wang, Y., Chen, D., Han, J., Zhang, Y., and Zhao, Z. (2022). Multimodal-based weld reinforcement monitoring system for wire arc additive manufacturing. *Journal of Materials Research and Technology*, 20:561–571.

Tan, M. and Le, Q. (2019). EfficientNet: Rethinking model scaling for convolutional neural networks. In Chaudhuri, K. and Salakhutdinov, R., editors, *Proceedings of the 36th International Conference on Machine Learning*, volume 97 of *Proceedings of Machine Learning Research*, pages 6105–6114. PMLR.

Zhu, Q., Liu, Z., and Yan, J. (2021). Machine learning for metal additive manufacturing: predicting temperature and melt pool fluid dynamics using physics-informed neural networks. *Computational Mechanics*, 67(2):619–635.